Reliability Assessment on Deep Braced Excavations Adjacent to High Slopes in Mountain Cities

R. H. Zhang[1], W. G. Zhang[1 and 2], Z. J. Hou[1], and W. Wang[1]
[1]*School of Civil Engineering, Chongqing University, Chongqing, China*
[2]*Key Laboratory of New Technology for Construction of Cities in Mountain Area, Chongqing University, Chongqing, China*
E-mail: cheungwg@126.com

ABSTRACT: Due to rapid urbanization, the land available for city construction and development becomes more and more scarce. Within a built-up environment, the construction safety of a deep excavation becomes more crucial with the ever-increasing building density. For deep excavations in mountain cities, the areas of the foundation pit to be excavated are generally the passive soil pressure zones for the upper existing slope. Construction disturbance, weakening of the passive area, as well as the formation of even higher slope through the superposition of foundation pit to the existing upper slope, will result in more deformation and even failure of the slope. This study numerically investigates the influences of excavation geometries, the system stiffness and the distance between the excavation and slope and develops simplified ultimate and serviceability limit state surrogate models with regard to the overall factor of safety and the maximum lateral wall deflection of the supporting system, respectively. Considering the uncertainties of the design parameters, a probabilistic framework combining the estimation models with First-Order Reliability Method (FORM) is proposed to determine the probability that a threshold factor of safety or the pre-defined maximum wall deflection is exceeded. The study presents preliminary guidelines for reliability assessment of ultimate and serviceability limit state designs for deep braced excavations adjacent to high slopes in mountain cities.

KEYWORDS: Braced excavation, Upper slope, Wall deflection, Factor of safety, Reliability assessment.

1. INTRODUCTION

With the promotion of the Belt and Road Initiatives in China, the fast urbanization progress has brought the great demand of commodity housing and public transport facilities. Thus, it is inevitable that more deep excavations to be constructed for residence, commercial buildings as well as the skyscrapers designed aside the existing slopes in densely populated mountainous cities such as Hongkong, Chongqing and Guiyang. It is well known that for deep excavations in mountain cities, the areas of the foundation pit to be excavated are generally also the passive soil pressure zones for the upper existing slopes. Consequently, the construction disturbances, weakening of the passive area, as well as the formation of the even higher slope through superposition of foundation pit to the existing upper slope, will result in more deformation and even collapse of the slope. Nevertheless, there are few investigations of the interaction between braced excavation and the adjacent slope and the influence of such interaction on the overall stability. Li et al. (2011) investigated the stability of supporting system and the safety of deep braced excavation adjacent to slope, through analyzing the influence of excavation of Shangshuijing station Shenzhen Metro Line 5 on side slope using FLAC3D. Wang et al. (2011) examined the deformation characteristics and behaviors of retaining structures for a complex geotechnical system comprising of a high building slope and a nearby deep excavation, based on field instrumentations. Varzaghani and Ghanbari (2014) presented a new analytical model to determine the seismic displacements of the shallow foundations adjacent to slopes. However, there is still a lack of systematic investigation of the key influential factors and the effects on the ultimate limit state and serviceability limit state of the excavation and slope system.

In this study, the global factor of safety *FS* obtained via the shear strength reduction (SSR) technique (also called *c/φ* reduction method) is used as the criterion for the ultimate limit state and the calculated maximum lateral wall deflection is adopted as the serviceability limit state criterion. It then numerically investigates the influences of the excavation geometries, the supporting system stiffness, the distance between the new excavation and the existing slope on excavation responses including the global *FS* and the wall deflection using PLAXIS software. Estimation models with regard to both the ultimate and serviceability limit states are developed. Probabilistic framework combining the proposed estimation models with the First-Order Reliability Method (FORM) is adopted to determine the probability that a threshold factor of safety or the maximum wall deflection is exceeded. This proposed approach enables a cost-effective analysis to be conducted for a rational design of excavation system adjacent to an existing high slope.

2. FINITE ELEMENT ANALYSIS

2.1 Numerical modelling

The PLAXIS^{2D} software was utilized for the numerical simulations. The Mohr-Coulomb constitutive model was selected for the soil. A typical cross-section of the excavation and slope system, the geometries as well as the properties of the soil and the supporting elements are shown in Figure 1. Apart from Figure 1, the soil properties include: dilation angle ψ = 5°, and unit weight γ = 19.0 kN/m^3.

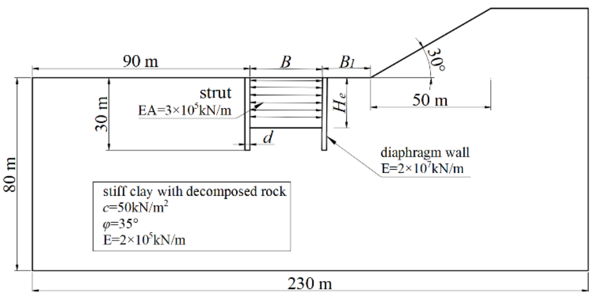

Figure 1 Cross-sectional soil and wall profile

The analyses considered a plane strain excavation supported by a retaining wall system near an unreinforced slope. The soil was modeled by 15-noded triangular elements. The structural elements were assumed to be linear elastic with the wall represented by 5-noded beam elements and 3-noded bar elements were used for the 6 levels of struts located at depths of 1 m, 4 m, 7 m, 10 m, 13 m and 16 m below the original ground surface, respectively. The nodes along the side boundaries of the mesh were constrained from displacing horizontally while the nodes along the bottom boundary were constrained from moving horizontally and vertically. The left and right vertical boundary extend far from the excavation to minimize the effects of the boundary restraints. The ranges of design parameters are shown in Table 1.

The strut stiffness per meter EA is assumed as a constant at 3.0×10^5 kN/m since the influence of strut stiffness on wall deflection is not very significant when the strut is stiff (Poh and Wong 1997, Zhang et al. 2015, Goh et al. 2017a,b, Zhang et al. 2019, Goh et al.2020, Li and Zhang 2020, Zhang et al. 2021). A total of 162 hypothetical cases were analysed.

The construction sequence comprised the following steps:

(1) the wall is installed ("wished into place") without any disturbance to the surrounding soil;
(2) the soil is excavated uniformly 1 m below each target strut level prior to adding the strut support with struts at 3 m vertical spacing until the final depth H_e is reached.
(3) Each phase of strut installation is followed by a subsequent phase of global safety factor calculations by SSR method.

Details are listed in Table 2.

Table 1 Parameters considered and the ranges

Parameters	**Ranges**
*System stiffness *S*	3.794, 4.605, 5.187
Excavation width *B* (m)	20, 30, 40
Excavation depth H_e (m)	14, 17, 20
Wall thickness *d* (m)	0.6,0.9,1.2
Distance between braced excavation and side slope B_1 (m)	5,10,15,20,30,40
Penetration ratio D/H_e	0.50, 0.76, 1.14

* Influence of wall stiffness was studied by varying wall thickness d while keeping the Young's modulus of the wall constant (E = 1.20×10^6 kN/m^2). The corresponding natural logarithm of the system stiffness $S = \ln(EI/\gamma_w h^4_{avg})$, or the wall thickness of 0.6, 0.9 and 1.2 m with average vertical strut spacing h_{avg} = 3 m. It should be noted that S is dimensionless.

Table 2 Construction procedures

Phases	**Construction details**
Initial Phase	Generate the initial effective stress, pore pressure and state parameters.
Phase 1	Calculated the global safety factor by SSR method
Phase 2	Install the diaphragm wall
Phase 3	Reset displacement to zero, excavate to 2 m below the ground surface (BGS) inside the excavation, install strut at 1 m BGS
Phase 4	Excavate to 5 m BGS
Phase 5	Install strut at 4 m BGS
Phase 6	Calculated the global safety factor by SSR method
Phase 7	Excavate to 8 m BGS
Phase 8	Install strut at 7 m BGS
Phase 9	Calculated the global safety factor by SSR method
Phase 10	Excavate to 11 m BGS
Phase 11	Install strut at 10 m BGS
Phase 12	Calculated the global safety factor by SSR method
Phase 13	Excavate to 14 m BGS
Phase 14	Install strut at 13 m BGS
Phase 15	Calculated the global safety factor by SSR method
Phase 16	Excavate to 17 m BGS
Phase 17	Install strut at 16 m BGS
Phase 18	Calculated the global safety factor by SSR method
Phase 19	Excavate to 20 m BGS
Phase 20	Calculated the global safety factor by SSR method

2.2 Numerical results

The numerical results include the factor of safety *FS* and the maximum lateral wall deflection δ_{hm}. *FS* is solved through SSR technique, in which the shear strengths are systematically reduced until failure occurs. This procedure was proposed by Zienkiewicz et al. (1975), and improved by Brinkgreve and Bakker (1991). It has been verified by Lian et al. (2001) that the SSR FE method can be widely applied in the engineering practice since this method takes advantages over the conventional limit equilibrium method. Cheng et al. (2007), Dawson et al. (1999), Gao et al. (2019) proved that the SSR technique perform well in many slope cases. Goh and Zhang (2012), Zhang and Goh (2015), Zhang et al. (2017), Goh et al. (2019), Zhang et al.(2020) adopted the SSR method for cavern stability analysis and basal heave analysis of deep braced excavations, respectively.

Figure 2 plots the variation of slip surface contours as excavation proceed, for case of B = 30 m, B_1 = 5 m, S = 4.605. The *FS* values for excavation depths H_e of 0, 14, 17, 21 m are also calculated, respectively. It can be observed that as excavation proceeds, *FS* values decrease. The smallest *FS* is about 1.705 with a decrease of 0.636 from the previous 2.341. In addition, it is also clear that a larger slip surface occurred when the excavation depth H_e becomes greater.

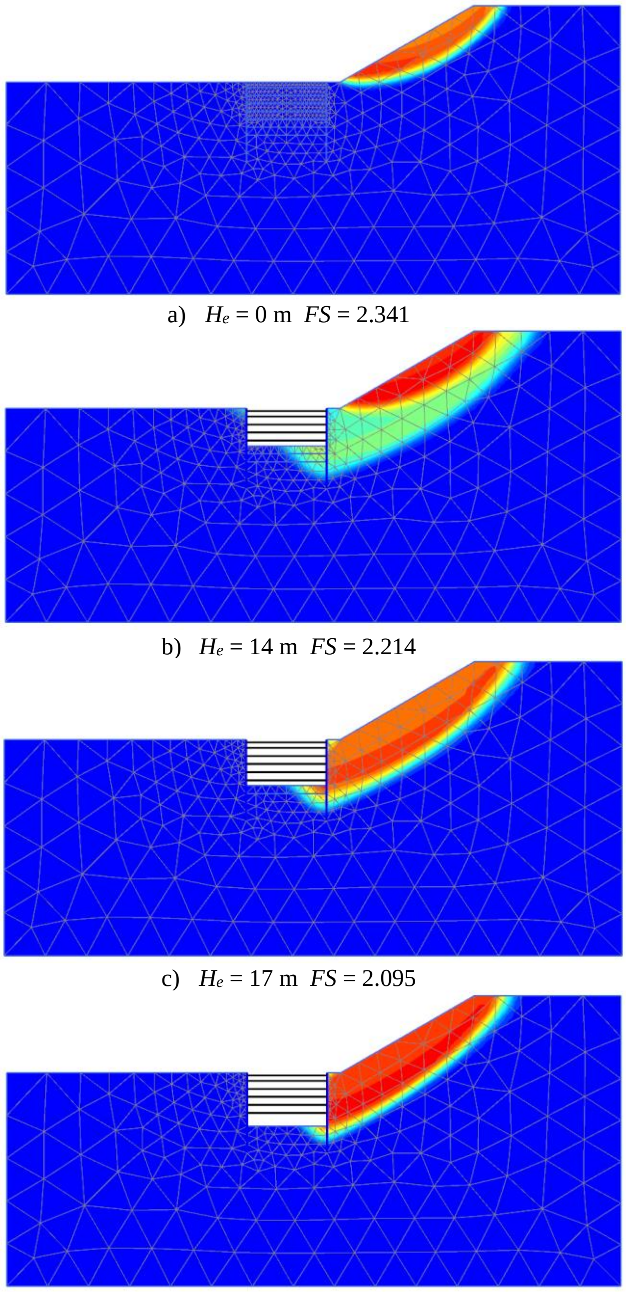

a) H_e = 0 m *FS* = 2.341

b) H_e = 14 m *FS* = 2.214

c) H_e = 17 m *FS* = 2.095

d) H_e = 20 m *FS* = 1.705

Figure 2 Contour of slip surface and *FS* for different excavation depths H_e with B = 30 m, B_1 = 5 m, and S = 4.605

Figure 3 presents some typical plots of the *FS* decrease for different B_1 for H_e = 20 m, S = 4.605. Generally, *FS* decrease becomes less significant as the distance between the excavation and the existing slope B_1 increases and converges to 0, indicating that the further away the excavation is from the existing upper slope, the much safer the whole system is. In addition, for the model dimensions considered in this study, the braced excavation has marginal impact on stability of the adjacent slope when the separation B_1 is greater than 40 m. As for the lateral deflections of the retaining wall on the slope side, Figure 4 shows the maximum lateral wall deflection δ_{hm} for different distances B_1 for case of H_e = 20 m, S = 4.605. It is clear that δ_{hm} has a tendency to grow with excavation width B while it decreases with increase of the separation B_1.

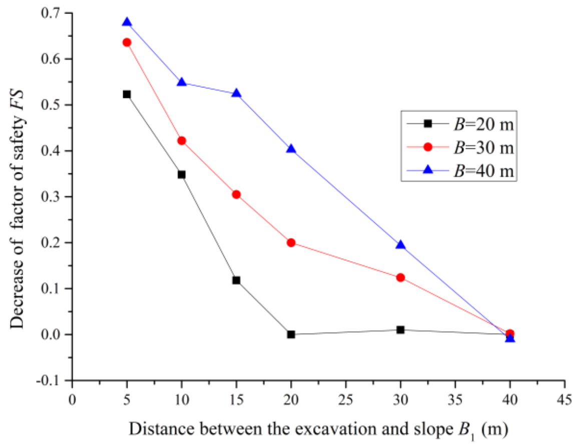

Figure 3 Decrease of factor of safety FS on different B_1 for H_e = 20 m, S = 4.605

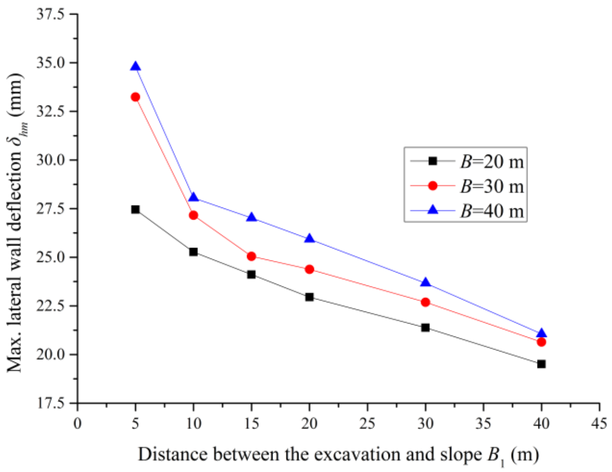

Figure 4 Max. lateral wall deflection δ_{hm} for different B_1 of case H_e = 20 m, S = 4.605

3. ESTIMATION MODELS FOR THE LIMIT STATE FUNCTIONS

For the performance in deep braced excavations, especially for the excavations adjacent to high slopes, both the ultimate limit state (ULS) and the serviceability limit state (SLS) should be satisfied. In the following sub sections, the limit state functions for ULS and SLS are developed respectively, based on the numerical results in the previous section.

3.1 Ultimate limit state model

Based on the calculated FS results, a Polynomial Regression (PR) model has been developed for estimating the factor of safety FS as a function of four input parameters: B, B_1, H_e and S in Eq. (1), with a coefficient of determination R^2 of 0.881, as below

$$FS = 7.35\times10^{-2}B - 1.57\times10^{-1}B_1 + 3.51\times10^{-2}H_e + 1.02S - 2.5\times10^{-6}B^2 - 2.29\times10^{-4}B_1^2 - 8.07\times10^{-4}H_e^2 - 2.22\times10^{-2}S^2 + 2.4\times10^{-4}BB_1 - 4.08\times10^{-3}BH_e + 1.65\times10^{-4}BS + 8.01\times10^{-3}H_eB_1 - 1.56\times10^{-3}SB_1 - 2.8\times10^{-2}H_eS - 1.84\times10^{-2}B(D/H_e) + 4.83\times10^{-2}B_1(D/H_e) + 9.4\times10^{-2}H_e(D/H_e) - 3.55\times10^{-1}S(D/H_e) \quad (1)$$

Figure 5 plots the estimated factor of safety $FS_{\_FEM}$ values against the calculated $FS_{\_EST}$ results. Also shown are the 100% agreement line and the 10% error lines, indicating that Eq. (1) is fairly accurate in predicting the global factor of safety for deep braced excavations adjacent to high slopes since the majority of data points are within the error lines.

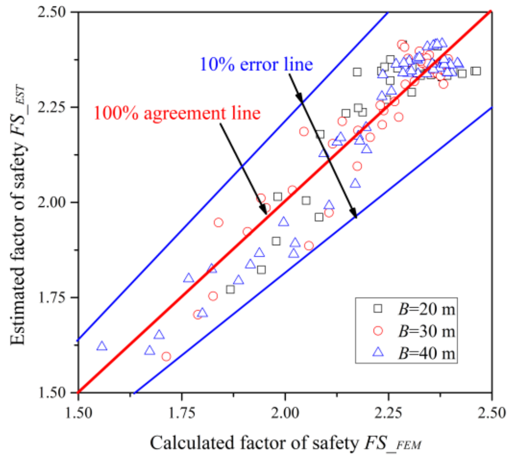

Figure 5 Comparison between $FS_{\_FEM}$ and $FS_{\_EST}$

3.2 Serviceability limit state model

Similarly, a Logarithmic Regression (LR) model for predicting the maximum lateral wall deflection δ_{hm} is developed and shown in Eq. (2), with fairly high coefficient of determination R^2 = 0.946, as below

$$\delta_{hm} = 0.1133B^{0.1086}B_1^{-0.223}(H_e)^{2.1247}(D/H_e)^{0.0568}S^{-0.4448} \quad (2)$$

Figure 6 plots the estimated maximum lateral wall deflections δ_{hm_EST} values against the calculated results δ_{hm_FEM}. Also shown are the 100% agreement line and the 20% error lines, indicating that Eq. (2) is fairly accurate in predicting the maximum wall deflections induced by deep braced excavations adjacent to high slopes.

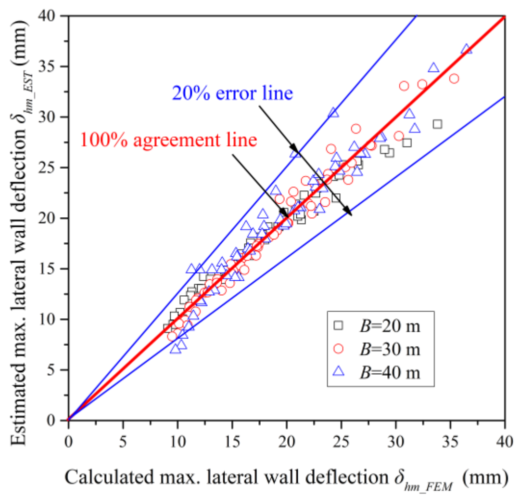

Figure 6 Comparison between δ_{hm_FEM} and δ_{hm_EST}

4. PROBABILISTIC ASSESSMENT OF THE LIMIT-STATES

In civil engineering applications, the assessment of safety is made by firstly establishing a relationship between the load S of the system and the resistance R. The boundary separating the safe and 'failure' domains is the limit state surface (boundary) defined by G(**x**) = R−S

= 0, where **x** is vector of the random variables. Mathematically, R > S or G(**x**) > 0 would denote a 'safe' domain. An unsatisfactory or 'failure' domain occurs when R < S or G(**x**) < 0. Calculation of P_f involves the determination of the joint probability distribution of R and S and the integration of the Probability Density Function (PDF) over the failure domain. Considering that the PDFs of the random variables are not known in most geotechnical applications and the integration is computationally demanding when multi-variables are involved, an approximate method, known as the First-Order Reliability Method (FORM) (Hasofer and Lind, 1974), is commonly used to assess the probability failure P_f. Low (1996) has shown that Microsoft EXCEL spreadsheet can be used to perform the minimization and determine reliability index β.

The reliability index β and the probability of failure P_f for both ULS and SLS can be performed using FORM based on the built PR and LR models. The ULS model Eq. (1) is incorporated into an EXCEL spreadsheet environment based on the approach by Low and Tang (2007), from which β can be determined. Figure 7 shows a sample spreadsheet for computing the factor of safety *FS* where the statistics of the design parameters are the same as those used in the previous section. The spreadsheet cells B3:B5 allow the selection of various distribution types for the input variables, including normal, lognormal, triangular etc., as explained in Low and Tang (2007). Nonnormal distributions are replaced by an equivalent normal ellipsoid, centred at the equivalent normal mean. Cells D3:E5 are parameters which are set corresponding to the normal distribution in this study. The correlation matrix R in cells G3:I5 are used to define the correlations between *B*, H_e and *S*. The n_i vector in cells J3:J5 contains equations for $(x_i - u_i^N) / \sigma_i^N$. The design point (x* values) was obtained by using the spreadsheet's built-in optimization routine SOLVER to minimize the cell, by changing the x* values, under the constraint that the performance function G(x*) = 0. Prior to invoking the SOLVER search algorithm, the x* values were set equal to the mean values (30, 17, 4.5) of the original random variables. Iterative numerical derivatives and directional search for the design point x* were automatically carried out in the spreadsheet environment.

Probabilistic assessment of SLS in Figure 8 is almost the same as Figure 7 except the G(x) formulations. For the detailed procedures in performing the FORM spreadsheet framework to derive β and the corresponding P_f, the paper published by Zhang and Goh (2012) can be referred to.

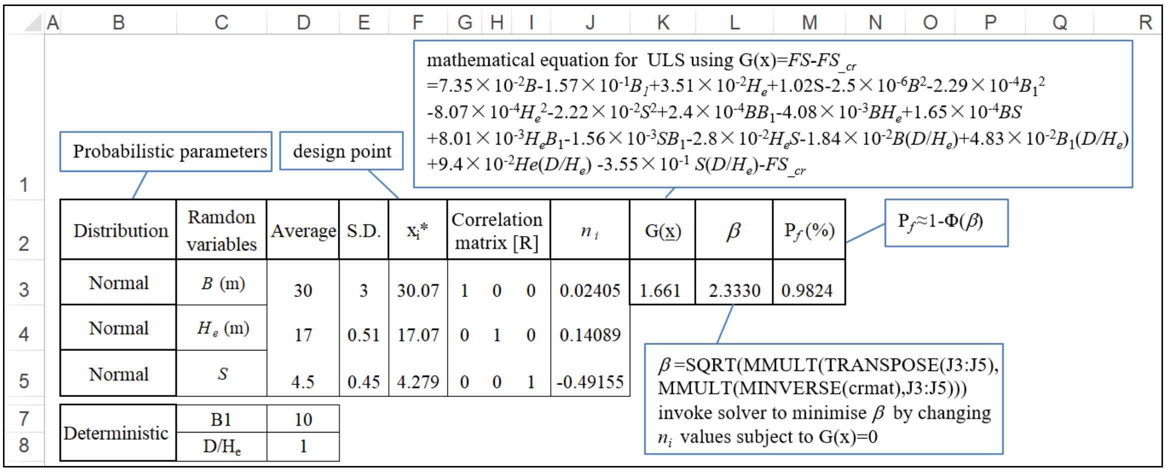

Distribution	Ramdon variables	Average	S.D.	x_i*	Correlation matrix [R]			n_i	G(x)	β	P_f(%)
Normal	*B* (m)	30	3	30.07	1	0	0	0.02405	1.661	2.3330	0.9824
Normal	H_e (m)	17	0.51	17.07	0	1	0	0.14089			
Normal	*S*	4.5	0.45	4.279	0	0	1	-0.49155			
Deterministic	B1	10									
	D/H_e	1									

Figure 7 Calculation on β and P_f for ultimate limit state using FORM spreadsheet

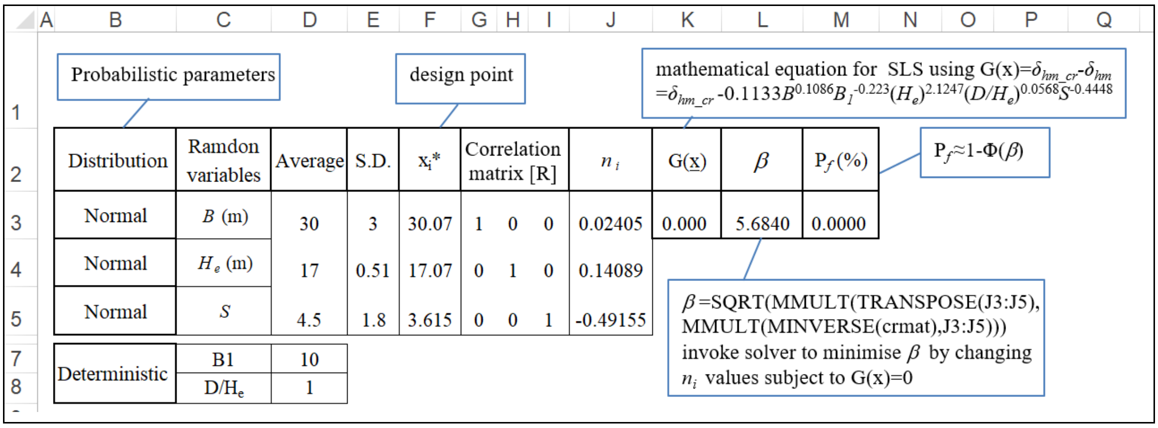

Distribution	Ramdon variables	Average	S.D.	x_i*	Correlation matrix [R]			n_i	G(x)	β	P_f(%)
Normal	*B* (m)	30	3	30.07	1	0	0	0.02405	0.000	5.6840	0.0000
Normal	H_e (m)	17	0.51	17.07	0	1	0	0.14089			
Normal	*S*	4.5	1.8	3.615	0	0	1	-0.49155			
Deterministic	B1	10									
	D/H_e	1									

Figure 8 Calculation on β and P_f for serviceability limit state using FORM spreadsheet

4.1 Probabilistic assessment of the ultimate limit state

For either the braced excavation or the slope, there are design code with regard to the choice of the critical factor of safety. However, for the excavation and slope system, there are no guidelines for the determination of such critical safety factor values. Thus the influence of the critical factor of safety *FS_cr* on β and P_f of ULS is examined in this study.

Figure 9 plots the influence of the various design parameters on the β and P_f of ULS. It is clear that both the coefficient of variation (COV, defined as the ratio of the standard deviation to the average mean value, i.e., COV = S.D. /Average) of the system stiffness COV_S and the critical factor of safety *FS_cr* significantly influence the β and P_f. In addition, the influence of COV_S on β and P_f is also as significant as that for *FS_cr*. The plots in Figure 10 indicate that the influence of either B_1 or COV_S on β and P_f is also significant when different excavation widths *B* of 20, 30, 40 m are considered.

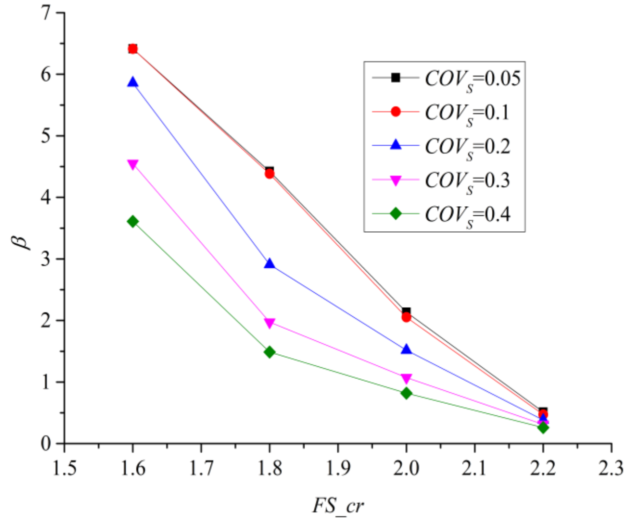

(a) (b)

Figure 9 Influence of COV_S and FS_cr on a) β and b) P_f for B_1 = 5 m, B = 30 m, H_e = 17 m, S = 4.5

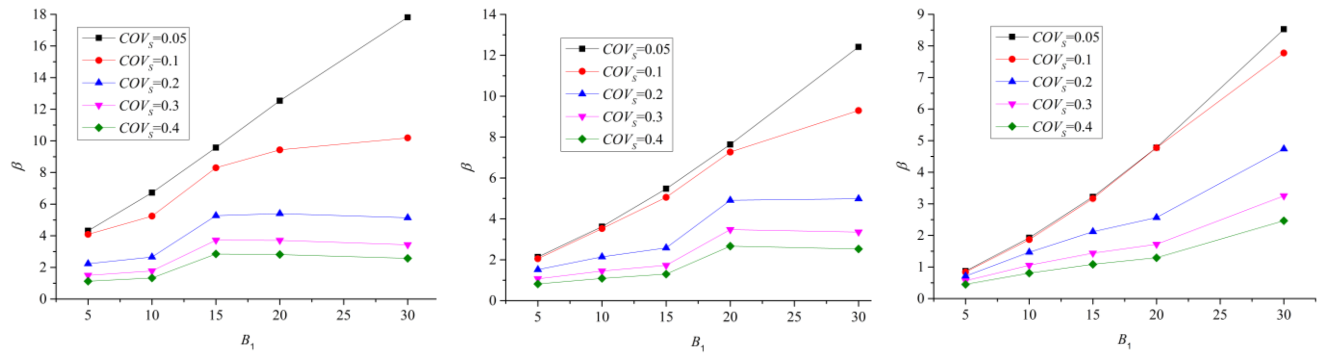

B = 20 m B = 30 m B = 40 m

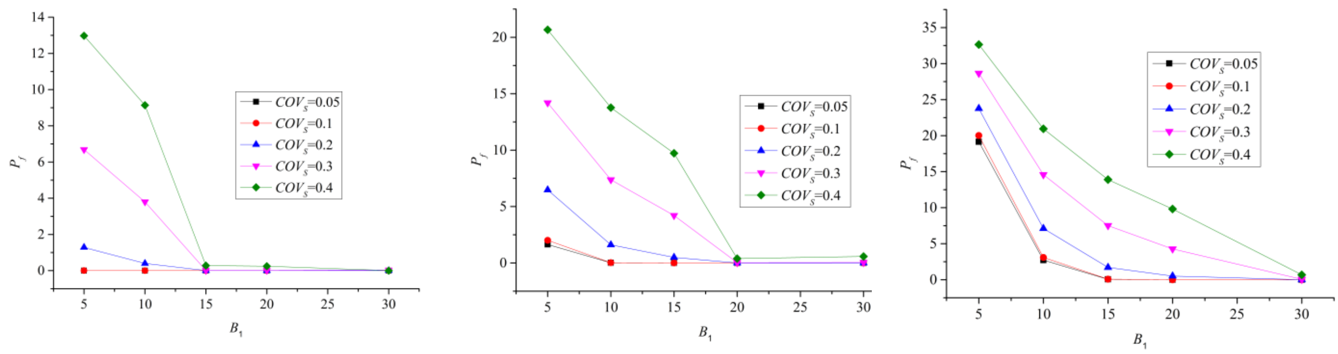

B = 20 m B = 30 m B = 40 m

Figure 10 Influence of COV_S and B_1 on β and P_f for B = 20, 30, 40 m, H_e = 17 m, S = 4.5, FS_cr = 2.0

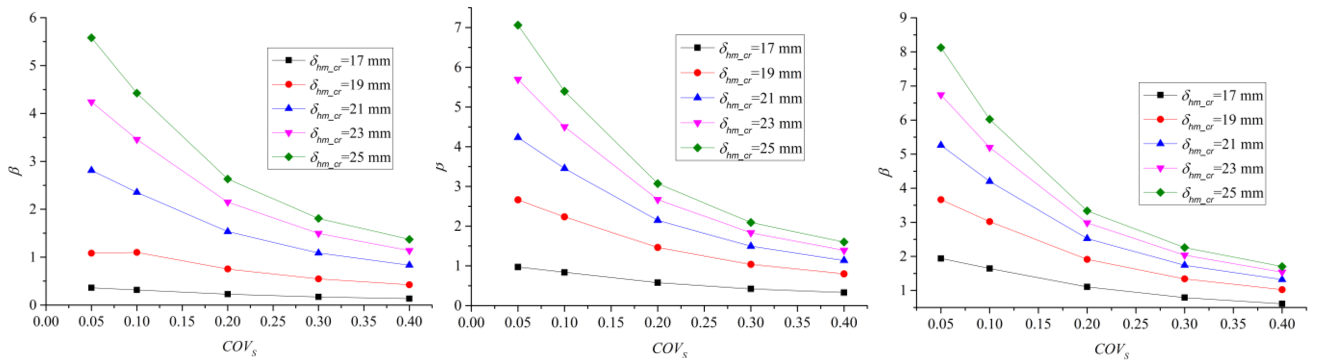

B_1 = 20 m B_1 = 30 m B_1 = 40 m

Figure 11 Influence of COV_S and δ_{hm_cr} on β for B = 30 m, H_e = 17 m, S = 4.5, B_1 = 20, 20, 40 m

Figure 10 also compares the influence of both the COV_S and B_1 on β and P_f for B = 20, 30, 40 m, respectively, with H_e = 17 m, S = 4.5, and FS_cr = 2.0. It is obvious that β becomes greater with increase of the excavation width B_1 while decreases with the increase of excavation width B. Meanwhile, P_f decreases as the excavation becomes further away from the slope. A greater excavation width B generally results in a larger P_f. Generally P_f converges to 0 when the separation is sufficient. However, different B causes different convergence speeds.

4.2 Probabilistic assessment of the serviceability limit state

There are also discussions as for the choice of the threshold lateral wall deflections for serviceability considerations (Zhang et al. 2018). Figure 11 plots the influence of COV_S and the critical max. wall deflection δ_{hm_cr} on β and P_f for B = 30 m, H_e = 17 m, S = 4.5 and B_1 = 20, 20, 40 m, respectively, indicating that both COV_S and δ_{hm_cr} significantly influence the β and P_f. However, the influence of COV_S on β and P_f is not as significant as that for δ_{hm_cr}, especially when COV_S is greater than 0.20. β has a tendency to grow with the critical maximum lateral wall deflections δ_{hm_cr} since the probability that a greater threshold is exceeded is much lower. β decreases with the increase of COV_S. In addition, it can be observed that the influence of B_1 on β is also significant since β increases substantially with the separation B_1.

Figure 12 shows the influence of COV_S on β for H_e = 17 m, S = 4.5, δ_{hm_cr} = 23 mm, B = 20,30, 40 m and B_1 = 10,15 m respectively. It is clear that β decreases as the variation of the system stiffness becomes greater. It is logical that β increases when the excavation is becoming further away from the slope.

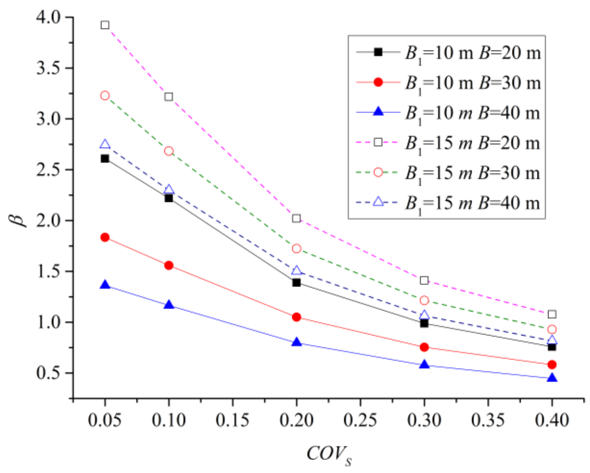

Figure 12 Influence of COV_S on β for H_e = 17 m, S = 4.5, δ_{hm_cr} = 23 mm, B = 20,30, 40 m and B_1 = 10,15 m

5. SUMMARY AND CONCLUSIONS

This paper presents numerical investigations about influence of braced excavation on the existing upper slope, from perspectives of the global factor of safety and the maximum lateral wall deflections. It also proposed probabilistic framework for quantitative assessment of both ULS and SLS in view of some design and construction uncertainties.

Regression models for the ultimate and serviceability limit states are developed respectively. Through the use of the automated spreadsheet search algorithm to determine the design point, to meet the different target performance levels, the critical FS or the threshold max. lateral wall deflection can be obtained. The influences of the key parameters, as well as the design uncertainties on the reliability index and the probability failure are examined. The framework and procedures outlined in this paper can be used to obtain a rational design of braced excavation adjacent to high slope and a cost-effective analysis.

6. ACKNOWLEDGEMENTS

The authors are also grateful to the financial support from National Natural Science Foundation of China (No. 52078086), Program of Distinguished Young Scholars, Natural Science Foundation of Chongqing, China (cstc2020jcyj-jq0087) and Innovation Group Science Fundation of the Natural Science Fundation of Chongqing, China (Grant No.cstc2020jcyj-cxttX0003).

7. REFERENCES

Brinkgreve, R.B.J., and Bakker, H.L. (1991) "Non-linear finite element analysis of safety factors", In: Proc. 7th Int. Conf. on Computer Methods and Advances in Geomechanics, vol. 23, pp1117–1122.

Cheng, Y. M., Lansivaara, T., and Wei, W. B. (2007) "Two-dimensional slope stability analysis by limit equilibrium and strength reduction methods", Computers and Geotechnics 34(3), pp137-150.

Dawson, E. M., Roth, W. H., and Drescher, A. (1999) "Slope stability analysis by strength reduction", Geotechnique 49(6), pp835-840.

Gao, X., Liu, X., Zhang, W., Wang, W., and Wang, Z. (2019) “Influences of reservoir water level drawdown on slope stability and reliability analysis”, Georisk, 13(2), pp145-153.

Goh, A.T.C, Zhang, F., Zhang, W., Zhang, Y.M., and Liu, H. (2017a) “A simple estimation model for 3D braced excavation wall deflection”, Computers and Geotechnics 83, pp106-113.

Goh, A.T.C., Zhang, F., Zhang, W.G., and Otard, C.Y.S. (2017) “Assessment of strut forces for braced excavation in clays from numerical analysis and field measurements”, Computers and Geotechnics 86, pp141-149.

Goh, A.T.C., and Zhang, W.G. (2012) “Reliability assessment of stability of underground rock caverns”, International Journal of Rock Mechanics and Mining Sciences 55, pp157-163.

Goh, A.T.C., Zhang, W., and Wong, K.S. (2019) “Deterministic and reliability analysis of basal heave stability for excavation in spatial variable soils”, Computers and Geotechnics, 108, pp152-160.

Goh, A.T.C., Zhang, R.H., Wang, W., Wang, L., Liu, H., and Zhang W.G. (2020) “Numerical study of the effects of groundwater drawdown on ground settlement for excavation in residual soils”, Acta Geotechnica 15, pp1259–1272.

Hasofer, A.M., and Lind, N. (1974) "An exact and invariant first-order reliability format", J. Eng. Mech. ASCE 100 (1), pp111–121.

Li, Y. H., Liu, P. Liu, J, and Han, X. F. (2011) "Stability and Safety Analysis of Braced Excavation for Subway Station during Construction under the Condition of Side Slope", Applied Mechanics and Materials 99-100, pp1166-1170.

Li, Y, and Zhang, W. (2020) “Investigation on passive pile responses subject to adjacent tunnelling in anisotropic clay”, Computers and Geotechnics. https://doi.org/10.1016/j.compgeo.2020.103782

Lian, Z., Han, G., and Kong, X. (2001) "Stability analysis of excavation by strength reduction FEM", Chinese Journal of Geotechnical Engineering 23(4), pp407-411.

Low, B.K. (1996) "Practical probabilistic approach using spreadsheet", In: Shackelford, C.D., Nelson, P.P., Roth, M.J.S. (Eds.), Uncertainty in the Geologic Environment, GSP 58. ASCE, Reston, pp1284–1302.

Low, B.K., and Tang, W.H. (2004) "Reliability analysis using object-oriented constrained optimization.", Struct. Saf., 26(1), pp69-89.

Low, B.K., and Tang, W.H. (2007) "Efficient spreadsheet algorithm for first-order reliability method", J.Eng. Mech. ASCE, 133(12), pp1378-1387.

Poh, T.Y., Wong, I.H., and Chandrasekaran, B. (1997) "Performance of two propped diaphragm walls in stiff residual soils", Journal of Performance of Constructed Facilities, 11(4), pp190–199.

Varzaghani, M. I., and Ghanbari, A. (2014) "A new analytical model to determine dynamic displacement of foundations adjacent to slope" Geomechanics and Engineering, pp561-575.

Wang, Q. Y., Gu, D. P., Zhang, J. S., and Xiong, Z. B. (2011) "Analysis of slip-risk and dynamic monitoring of a high building slope fringed a deep foundation pit", Journal of safety and environment, 11(2), p6 (in Chinese).

Zhang W., and Goh, A.T.C. (2015) "Regression models for estimating ultimate and serviceability limit states of underground rock caverns" Engineering Geology 188, pp68-76.

Zhang, W., and Goh A.T.C. (2012) "Reliability assessment on ultimate and serviceability limit states and determination of critical factor of safety for underground rock caverns", Tunnelling and Underground Space Technology 32: pp221-230.

Zhang, W, and Goh A.T.C., and Xuan, F. (2015) "A simple prediction model for wall deflection caused by braced excavation in clays", Computers and Geotechnics 63, pp67-72.

Zhang, W., Zhang, Y., and Goh, A.T.C. (2017) "Multivariate adaptive regression splines for inverse analysis of soil and wall properties in braced excavation", Tunneling and Underground Space Technology 64, pp24-33.

Zhang, W., Goh, A.T.C., Goh, K.H., Chew, O.Y.S., Zhou, D., and Zhang, R. (2018) "Performance of Braced Excavation in Residual Soil with Groundwater Drawdown", Underground Space 3, pp150-165.

Zhang, W., Hou, Z., Goh, A.T.C., and Zhang, R. (2019) "Estimation of strut forces for braced excavation in granular soils from numerical analysis and case histories", Computers and Geotechnics, 106, pp286-295.

Zhang, W., Li, Y., Goh, A.T.C., and Zhang, R. (2020) "Numerical study of the performance of jet grout piles for braced excavations in soft clay", Computers and Geotechnics. https://doi.org/10.1016/j.compgeo.2020.103631.

Zhang, R., Wu, C., Goh, A.T.C., Böhlke, T., and Zhang, W. (2021) "Estimation of Diaphragm Wall Deflections for Deep Braced Excavation in Anisotropic Clays Using Ensemble Learning", Geoscience Frontiers. 12, pp365–373

Zienkiewicz, O.C., Humpheson, C., and Lewis, R. (1975) "Associated and non-associated visco-plasticity in soil mechanics", Geotechnique 25 (4), pp671–689.